International Journal of
Organizational Innovation

INFLUENCE OF STRAIN SOFTENING AND SHEAR-BAND TILTING EFFECTS ON THE ACTIVE EARTH PRESSURE ON RETAINING WALLS

Tse-Shan Hsu
President, Institute of Mitigation for Earthquake Shear Banding Disasters
Professor, Department of Civil Engineering, Feng-Chia University, Taiwan R.O.C.
tshsu@fcu.edu.tw

Yi-Ju Chen
Ph.D. Student, Ph.D. Program of Mechanical and Aeronautical Engineering,
Feng-Chia University, Taiwan, R.O.C.

Zong-Lin Wu   Yi-Lang Hsieh
Directors, Institute of Mitigation for Earthquake Shear Banding Disasters,
Taiwan R.O.C.

Jiann-Cherng Yang   Yi-Min Huang
Associate and Assistant Professors, Feng-Chia University, Respectively,
Taiwan, R.O.C.

Abstract

Local shear bands develop on highway slopes and river banks where retaining walls are located, and shear banding implies strain softening and shear-band tilting effects. However, the traditional theory of active earth pressure for retaining walls ignores the influence of shear-banding. As a result, design codes have not fortified against shear-banding, which has caused a large number of retaining walls under shear banding to collapse. In view of this, this paper explores the influence of strain softening and shear-band tilting effects on the maximum lateral earth pressure on a retaining wall. The results of this paper lead to the following four conclusions. (1) The main cause for collapse of shear-band retaining walls is that design codes do not for-

45

tify against shear banding. (2) Finite-element analysis results show that shear bands can only appear in the elastic-plastic strain softening model. The traditional active earth pressure theory for retaining walls assumes that a failure surface exists according to the elastic-perfectly plastic model. (3) Because piping failure in a retaining wall only occurs locally in the shear band, piping failure analysis for retaining walls should use unsteady-state pipe flow instead of steady-state seepage flow. (4) The case study results show that both strain softening and shear-band tilting effects increase the maximum lateral earth pressure on the retaining wall beyond the values calculated using the traditional active earth pressure method. The total increase can be as high as 148.6%, which shows that this calculation discrepancy is a key factor in the collapse of the shear-band retaining walls. Based on these four conclusions, it is suggested that strain softening and shear-band tilting effect should be included in retaining wall design codes, so as to ensure that retaining walls do not undergo local collapse.

Keywords: strain softening, shear-band tilting effect, piping failure, earth pressure, retaining wall.

Introduction

Generally speaking, slopes and river valleys are caused by a shear-band tilting effect that appears locally in tectonic earthquakes, while tectonic earthquakes originate from continuous lateral compression of tectonic plates. When the strain goes deep into the plastic range, the tectonic plate loses its ellipticity (Hsu, 1987; Needleman and Tvergaard, 1983; Prevost, 1984; Rice, 1976; Rudnicki, J. W. and Rice, 1975; Valanis, 1989) as a result of strain softening, so shear bands are formed after the occurrence of localized deformation (as shown in Figure 1).

Figure 1. Shear bands formed in a tectonic plate as a result of localized deformation under lateral compression (Hsu, 2018).

During shear banding, because the friction resistance changes with time, the stick-slip phenomenon occurs repeatedly (see Figure 2). When stick occurs, the friction resistance increases, and the plate decelerates; when slip occurs, the friction resistance decreases, and the plate accelerates. Therefore, during shear banding, vibration occurs as a result of repeated cycles of deceleration and acceleration in the tectonic plates (shown in Figure 3).
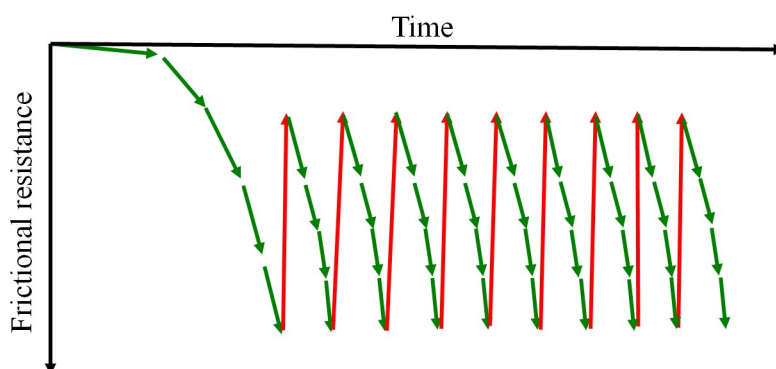

Figure 2. Repeated occurrence of stick-slip phenomena induced by friction resistance

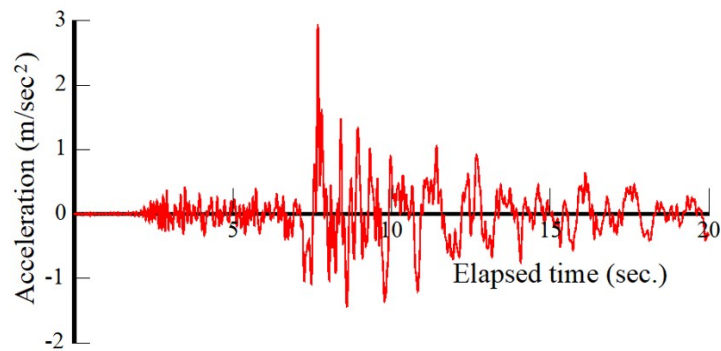(redrawn from Lambe and Whitman, 1969).

47

Figure 3. Acceleration versus time for ground vibrations induced by shear banding (Hsu, 2018).

There are five types of earthquakes (China Earthquake Disaster Prevention Center, 2019): tectonic earthquakes, volcanic earthquakes, subsidence earthquakes, reservoir storage-induced earthquakes, and artificial explosion-induced earthquakes, and the most common type are tectonic earthquakes. The main effect of tectonic earthquakes is shear banding, which accounts for more than 90% of the total energy, and a secondary effect is ground vibration, which only accounts for less than 10% of the total energy (Coffey, 2019). Because ground vibration is a temporary effect and shear banding continues to accumulate, the maximum lateral earth pressure on a retaining wall under shear banding increases with the increase in the strain softening and the uplifting effect of the soil behind the retaining wall. Even if the wall complies with existing design codes, it may still collapse in normal time (detailed in Figure 4), in heavy rain (detailed in Figure 5), and in earthquakes (detailed in Figure 6). Under these circumstances, the traditional design approach of scholars and technicians (Bowles, 1988; Chen, 1975; Coulomb, 1776) still ignores the influence of shear banding. This traditional approach assumes that a retaining wall will collapse under a maximum lateral earth pressure calculated using the elastic-perfectly plastic model. Therefore, current design codes do not fortify retaining walls against shear banding.

(a) Before collapse (Google Earth, 2010).

(b) After collapse (Water Resources Department Newsletter, 2018).

Figure 4. The 3.1K retaining wall on National Highway No. 3 collapsed in normal time.

Figure 5. A retaining wall in Lincoln County collapsed in heavy rain (New Taipei City Government, Taiwan, 1997).

Figure 6. A retaining wall in the Quanjiafu Community collapsed during the 921 Jiji earthquake in 1999 (Lian, 1999).

In view of this, in order to prevent the collapse of shear-band retaining walls, this paper first provides proof of the main cause of collapse of retaining walls. Then, analysis of the maximum lateral earth pressure based on the collapse mechanism for the proposed shear-band retaining wall is carried out to quantify the influence of strain softening and the shear-band tilting effect in the soil behind the retaining wall on the maximum lateral earth pressure exerted on the retaining wall.

Proof of the Main Cause of Collapse in Retaining Walls

Criteria for main cause of collapse of a retaining wall

If and only if the proposed cause for collapse of a retaining wall meets three criteria, including uniqueness, integrity, and comprehensiveness, then the proposed cause for collapse of a retaining wall is indeed the main cause of collapse of a retaining wall. The criteria are defined as follows:

1) Uniqueness

The retaining wall will only collapse under the conditions described in the proposed cause of collapse.

2) Integrity

When other retaining walls in the same area collapse with the same cause, the retaining wall in question should also collapse.

3) Comprehensiveness

When a retaining wall in one country collapses because of the proposed cause of collapse, other retaining walls in other countries in the world should also collapse under the same conditions.

Proof of the Main Cause for Retaining Wall Collapse

In addition to the collapse of the shear-band retaining wall shown in Figures 4 to 6, Figures 7 and 8 clearly show that the collapses of the retaining walls on a highway slope and river bank only occurred locally in the shear band zone.
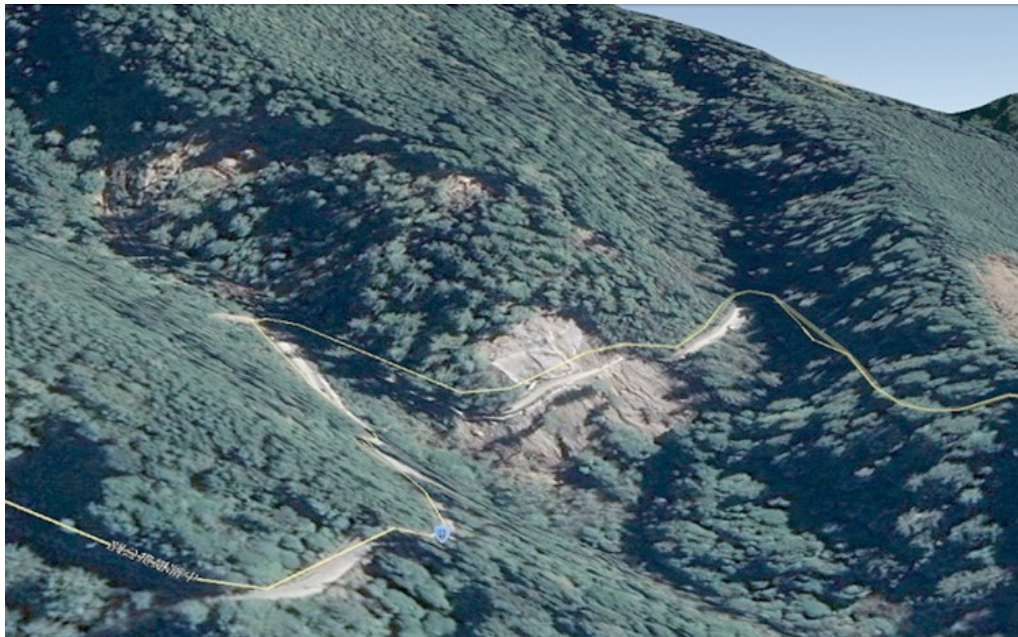
51

Figure 7. Local collapse of a retaining wall in a shear band zone on a highway slope (Tai-8 Route 109.5K, Central Transit Highway, Taiwan; Google Earth, 2010).

Figure 8. Local collapse of a shear-band retaining wall on a riverbank (right bank of the downstream Shigang Dam in Taiwan).

The lateral earth pressure on a retaining wall will increase with increasing degrees of brittle fracture in the soil behind the retaining wall, and this brittle fracture will increase with increasing amounts of shear banding. In this case, for a retaining wall that has met design codes, the cause of retaining wall collapse is proposed to be as follows: in the case that the design code has not fortified against shear banding, a retaining wall will collapse when the maximum lateral earth pressure increases excessively.

1) Proof of uniqueness

If the design code does not fortify against shear banding, then the maximum lateral earth pressure increases when strain softening or shear-band tilting effects occur in the soil behind the retaining wall. Therefore, the retaining wall will only collapse locally when the maximum lateral earth pressure increases past a specific threshold.

Only if the local collapse of the retaining wall is caused by an excessive increase in the maximum lateral earth pressure can the excessively large maximum lateral earth pressure be attributed to strain softening or shear-band tilting effects in the soil behind the retaining wall. Therefore, the

retaining wall will locally collapse only if the design code does not fortify against shear banding.

Therefore, the proposed cause of the collapse of the retaining wall satisfies the uniqueness criterion.

2) Proof of integrity

If the design code for a retaining wall in a certain area does not fortify against shear banding, then the local collapse of the retaining wall will be caused by an excessive increase in the maximum lateral earth pressure. Since the maximum lateral earth pressure increases only when the soil behind the retaining wall experiences strain softening or the shear-band tilting effect, other retaining walls in the same area will collapse locally under excessive maximum lateral earth pressure increases if they are also not fortified against shear banding.

Only if other retaining walls in the same area are not fortified against shear banding in the design code, then the local collapse will be caused by an excessive increase in the maximum lateral earth pressure. Since the maximum lateral earth pressure increases only when strain softening or shear-band tilting effects occur in the soil behind

53

the retaining wall, the retaining wall will locally collapse only if the design code does not fortify against shear-banding.

Therefore, the proposed cause of the collapse of the retaining wall satisfies the integrity criterion.

3) Proof of comprehensiveness

If retaining walls in various countries around the world are not built according to codes that consider shear banding, then these walls will experience local collapse when the maximum lateral earth pressure becomes excessively large. Since the maximum lateral earth pressure on a retaining wall only increases when the soil behind the retaining wall experiences strain softening or shear-band tilting effects, other retaining walls in various countries around the world will also collapse locally under similar excessive maximum lateral earth pressures when the design codes do not consider shear banding.

Only if other retaining walls in various countries around the world are not fortified against shear banding in the design code, then the local collapse will be caused by an excessive increase in the maximum lateral earth pressure. Since the maximum lateral earth pressure on a retaining wall will increase

only when strain softening or shear-band tilting effects occur in the soil behind the retaining wall, retaining walls in various countries around the world will locally collapse when the maximum lateral earth pressure is increased excessively because the design code does not fortify against shear banding.

Therefore, the proposed cause for the collapse of a retaining wall satisfies the comprehensiveness criterion.

Because it simultaneously meets all three criteria for cause of collapse, shear banding is concluded to be the main cause for the collapse of retaining wall.

Governing Equation for the Inclination Angle of a Coulomb Active Failure Surface

When a retaining wall moves to the left as a result of lateral compression, the failure block of the potential Coulomb active earth pressure (Coulomb, 1776) is ΔABC (detailed in Figure 9(a)). Here, H is the height of the retaining wall, γ is the unit weight of the soil, W is the weight per unit length of ΔABC, β is the inclination angle of $\overline{AC}$, θ is the inclination angle of $\overline{AB}$, ρ is the inclination angle of the potential active failure surface $\overline{BC}$,

54

$\rho - \beta$ is the angle between $\overline{CA}$ and $\overline{CB}$, R is the resultant shear-resisting force acting on $\overline{BC}$, the angle of intersection between R and line normal to $\overline{BC}$ is the internal friction angle ϕ,

P_a is the active earth pressure acting on $\overline{AB}$, and the angle of intersection between P_a and the normal of $\overline{AB}$ is the wall friction angle δ.
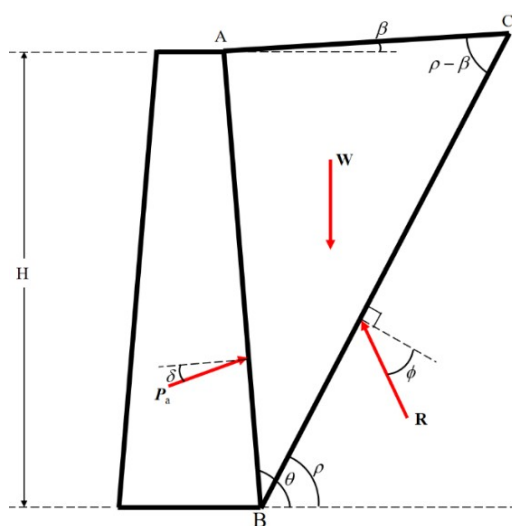
(a) Geometric conditions and acting forces.
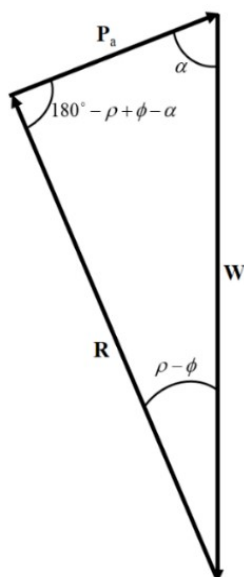
(b) Force polygon for the acting forces.

Figure 9. Geometric conditions, acting forces, and force polygon for Coulomb active earth pressure theory (Hsu et al., 2021).

For the Coulomb potential failure block ΔABC shown in Figure 9(a), the weight W is given by:

$$W = \frac{1}{2}\gamma H^2 \frac{\sin(\theta - \beta)}{\sin^2 \theta} \cdot \frac{\sin(\theta - \rho)}{\sin(\rho - \beta)} . \qquad \text{(Equation 1)}$$

Figure 9(b) is the force polygon of W, R, and P_a shown in Figure 9(a); under the balanced force conditions, the force polygon is closed, so Equation 2 can be obtained using the law of sines:

$$P_a = W \frac{\sin(\rho - \phi)}{\sin(180° - \rho - \alpha + \phi)}$$
$$= \frac{1}{2}\gamma H^2 \frac{\sin(\theta - \beta)}{\sin^2 \theta} \cdot \frac{\sin(\theta - \rho)}{\sin(\rho - \beta)} \cdot \frac{\sin(\rho - \phi)}{\sin(\rho + \alpha - \phi)} . \qquad \text{(Equation 2)}$$

When the inclination angle of the failure surface ρ is changed to maximize the value of P_a in Equation 2, P_a represents the Coulomb active earth pressure.

For non-cohesive soils, under the limit condition of the elastic-perfectly plastic model, the calculations of Coulomb active earth pressure consider the internal friction angle ϕ in Equation 2 to be constant; when β, θ, δ, $\alpha = 180° - \theta - \delta$, $\rho \neq \theta$, $\rho \neq \phi$, $\rho \neq \beta$, and $\rho \neq \phi - \alpha$ are known, the active earth pressure theorem can be applied. Hsu *et al*. (2021) presented a mathematical proof of the theorem and a governing equation that can be used to analyze the inclination angle of the failure surface under Coulomb active earth pressure:

$$\cot(\theta - \rho) + \cot(\rho - \beta) = \cot(\rho - \phi) - \cot(\rho + \alpha - \phi) . \qquad \text{(Equation 3)}$$

Test Methods and Results for Evaluation of the Maximum Lateral Earth Pressure on the Retaining Wall

Presently, there are a large number of retaining walls constructed in various countries around the world. Therefore, after Coulomb (1776) pro-

posed the theory of active earth pressure, other scholars (Ahire1 et al., 2019; Bowles, 1998; Chen, 1975; Sitar1 and Wagner, 2015; Terzaghi, et al., 1996; Choudhury, Deepankar and Chatterjee, 2006; Psarropoulosa, 2005) continue to conduct relevant research. However, in these traditional active earth pressure theories, the failure surface is assumed to appear under the limit state of elastic-perfectly plastic conditions.

Based on these assumptions, for non-cohesive soils, when solving for the inclination angle ρ of the Coulomb active failure surface using Equation 3, the internal friction angle ϕ

must be known.

On highway slopes or river banks, most of the soil behind retaining walls is not completely non-cohesive soil. Therefore, the soil experiences strain softening behavior after the strain goes deep into the plastic range. When undisturbed specimens are subjected to a triaxial compression test or a direct shear test in the laboratory, they can be tested under three different confining pressures σ_c and the test results have peak shear stress τ_p and residual shear stress τ_r (detailed in Figure 10).
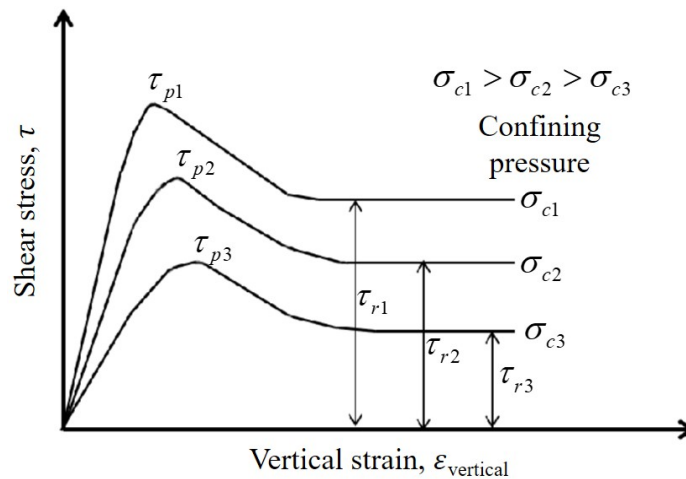
(a) Shear stress vs vertical strain for triaxial compression test.
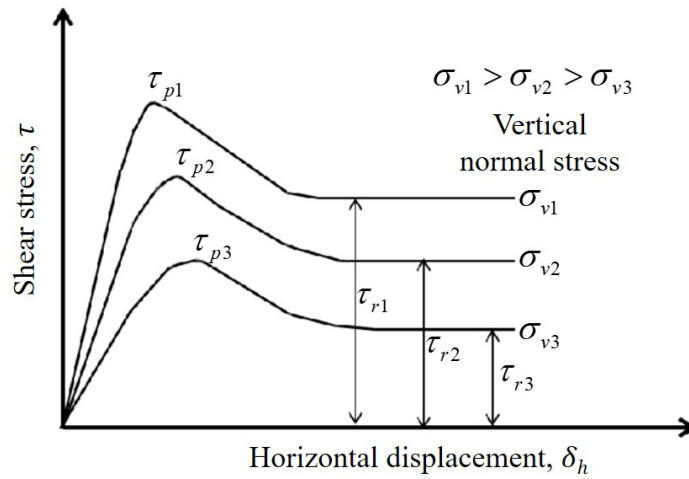
(b) Shear stress vs horizontal displacement for direct shear test.

Figure 10. Schematic diagrams of the test results for the triaxial compression test and the direct shear test.

According to Figure 10, under different confining pressures σ_c during the triaxial compression test or under different vertical stresses σ_v during the direct shear test, the peak shear stress τ_p and the residual shear stress τ_r can be calculated. Using these values, graphs illustrating the relationships between τ_p, τ_r, and the normal stress σ can be drawn (detailed in Figure 11).
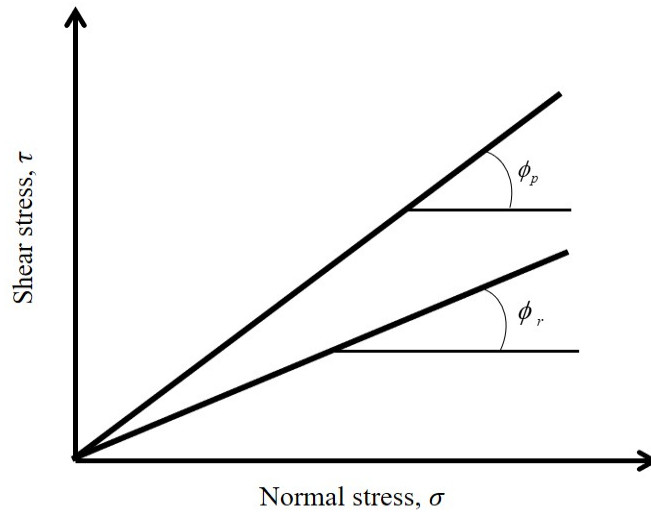
(a) Shear stress vs normal stress for cohesionless soil or fractured rock.
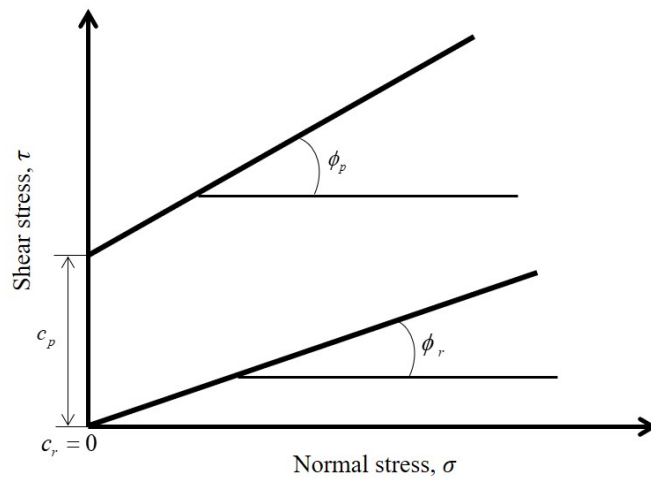
(b) Shear stress vs normal stress for cohesive soil or non-fractured rock.

Figure 11. Schematic diagrams of the peak and residual shear resistance strength parameters obtained from a triaxial compression test and a direct shear test.

Figure 11(a) shows the peak internal friction angle ϕ_p and the residual internal friction angle ϕ_r for non-cohesive soil, while Figure 11b

shows the peak internal friction angle ϕ_p, the peak cohesion c_p, the residual internal friction angle ϕ_r, and the residual cohesion c_r for cohesive soil,

59

where $c_r = 0$.

According to the Coulomb active earth pressure theory, there must be an active failure surface, represented as $\overline{BC}$ in Figure 9(a). According to the literature, the active failure surface only occurs after the strain goes deep into the plastic range (Hsu, 1987; Needleman and Tvergaard, 1983; Prevost, 1984; Rice, 1976; Rudnicki, J. W. and Rice, 1975; Valanis, 1989) and strain softening behavior appears. Therefore, when Equation 3 is used to calculate the inclination angle of the Coulomb active failure surface, ρ, both the test

method and the test results must be carefully selected.

For a traditional triaxial compression test, since the specimen is cylindrical and the specimen is sheared by applying vertical pressures, the failure surface (detailed in Figure 12) observed in the test specimen is obviously different from the failure surface $\overline{BC}$ in the soil behind the retaining wall (detailed in Figure 9(a)).
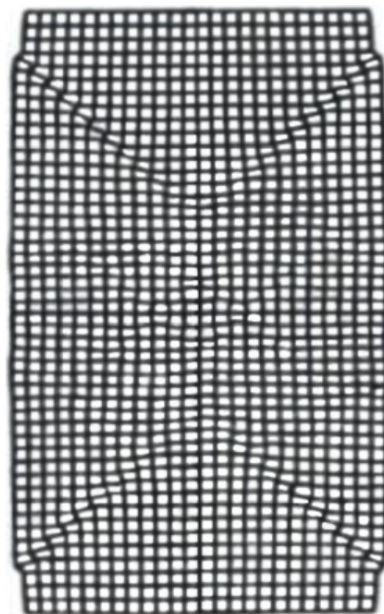

Figure 12. Typical failure surface obtained from a traditional triaxial compression test (Hsu, 1987).

In the direct shear test, a square   test specimen is subjected to horizontal

displacement by the upper or lower shear box. Therefore, the failure surface shown in Figure 13, which is obtained

in the direct test, is similar to the failure surface $\overline{BC}$ of the soil behind the retaining wall shown in Figure 9.
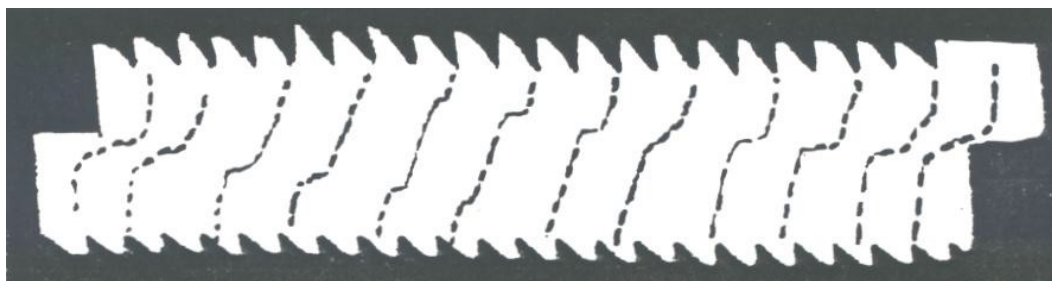

Figure 13. Typical failure surface obtained from a direct shear test (Hvorslev, 1961).

Secondly, for the shear-band retaining wall, when the Coulomb active failure surface is formed, the failure block will have principal deformation shear, thrust shear, Riedel shear, con-

jugate Riedel shear, and compression textures (detailed in Figure 14). During brittle fracture, the degree of brittle fracture in the failure block will increase with increased levels of sliding.
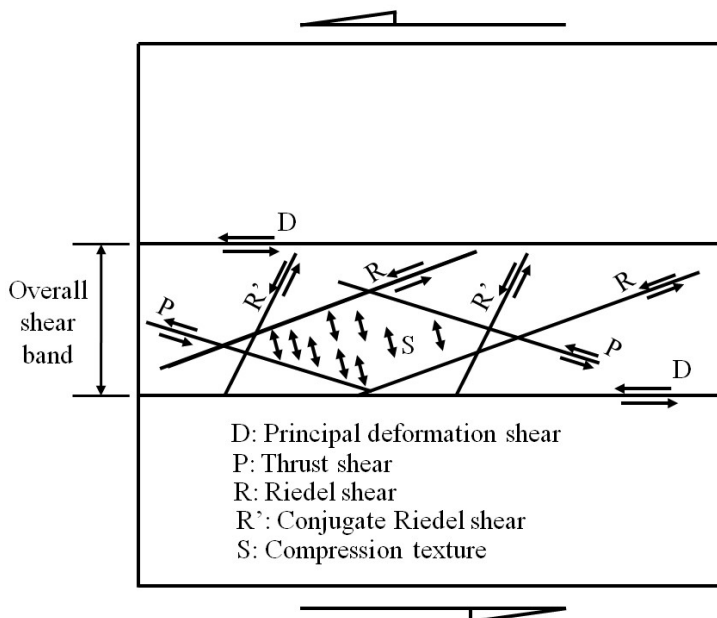

Figure 14. Various shear textures in the overall shear band (Tchalenko, 1968).

61

When strain softening occurs in the soil behind the retaining wall after the strain goes deep into the plastic range, the degree of brittle fracture in Coulomb's active failure block will be considerable. Therefore, even if the original soil behind the retaining wall is cohesive soil, its cohesive properties will disappear after brittle fracture. Thus, if the ac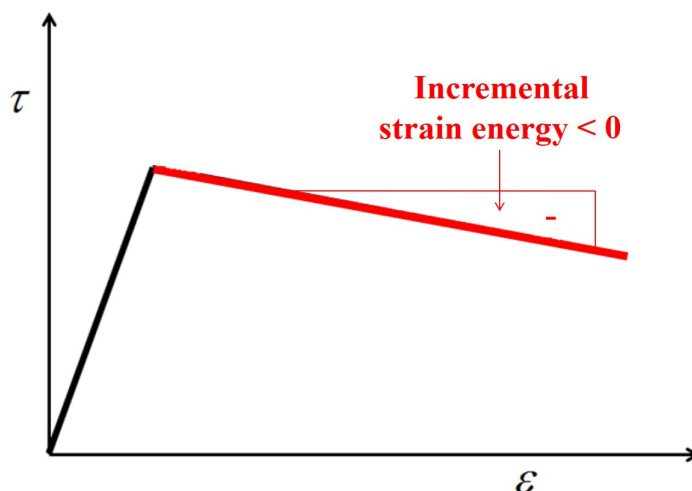tive earth pressure theory for the retaining walls uses the elastic-plastic strain hardening model (detailed in Figure 15(a)), or the elastic-perfectly plastic model (detailed in Figure 15(b)), the calculated behavior would be completely different from the real elastic-plastic strain softening behavior observed in the soil behind the retaining wall.
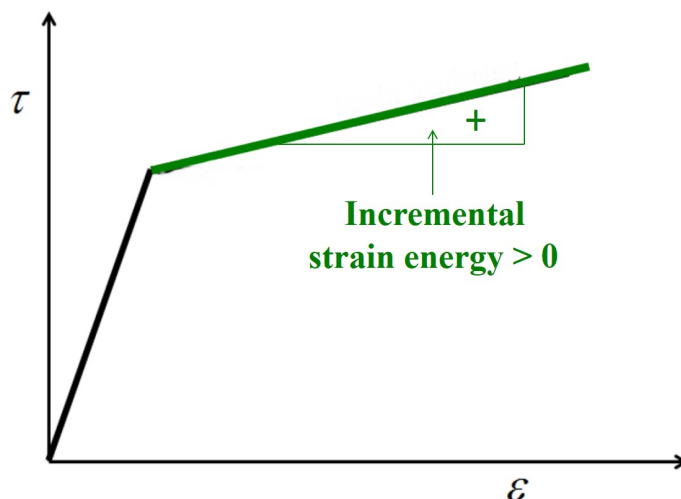
(a) Elastic-plastic strain hardening model.
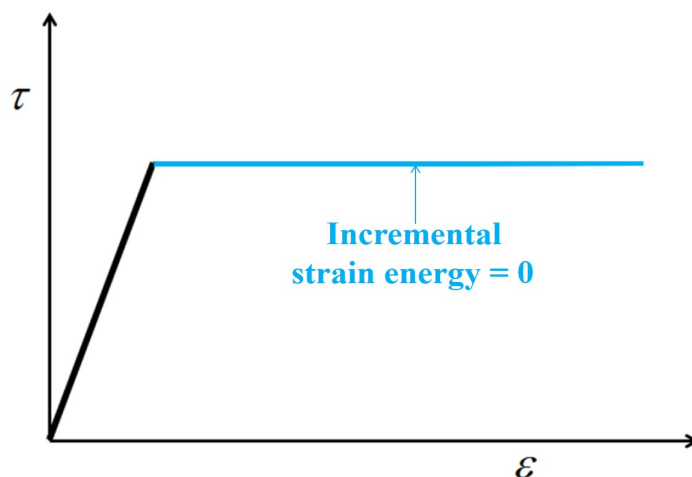
(b) elastic-perfectly plastic model.

(c) Elastic-plastic strain softening model.

Figure 15. Schematic diagrams of three different properties of soil models.

For the three different properties of soil models shown in Figures 15a to 15c, the numerical simulation analysis results from the finite-element simulations show that if the plane strain plate is under lateral compression and the strain is deep in the plastic range, then the plate does not develop shear bands for both the elastic-plastic strain hardening and elastic-perfectly plastic models (detailed in Figures 16(a) and 16(b)). The plate only develops shear bands in

63

the elastic-plastic strain softening model (detailed in Figure 16(c)).
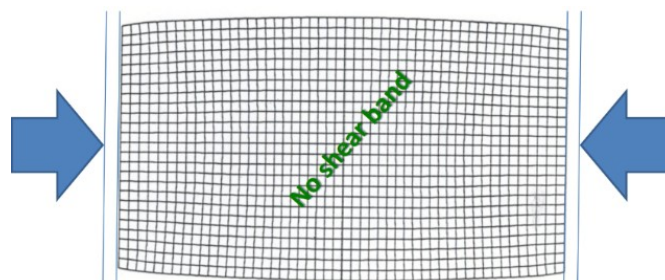
(a) No shear bands develop under the elastic-plastic strain hardening model.
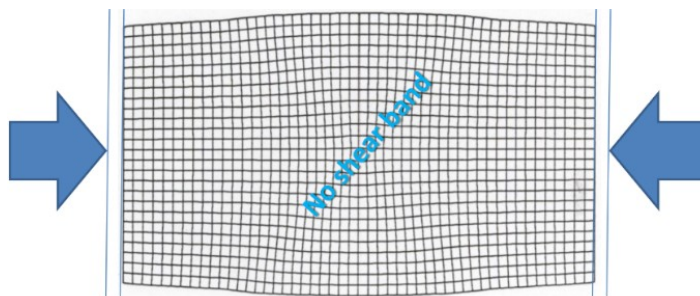
(b) No shear bands develop under the elastic-perfectly plastic model.
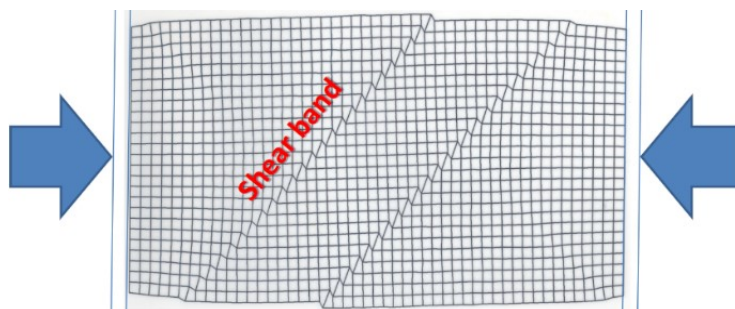
(c) Shear bands develop under the elastic-plastic strain softening model.

Figure 16. Finite-element simulation results for a plane strain plate under lateral compression after the strain goes deep into the plastic range (Hsu, 2019).

Figure 16 shows that the develop- ment of the failure surface requires two

conditions: strain softening and a strain that is deep in the plastic range. Strain softening originates from the volume expansion of a fractured block; thus, the negative strain energy increment (that is, the damage strain energy increment shown in Figure 16(c)) is the driving force that develops the failure surface.

The traditional theory of active earth pressure for retaining walls assumes that the stress-strain relationship is elastic-perfectly plastic. Thus, the volume remains unchanged after the strain goes into the plastic range, so the failure surface cannot be developed in the absence of damage strain energy.

Therefore, when it is necessary to evaluate the inclination angle ρ of the active failure surface for the retaining wall using Equation 3, it is recommended to conduct a direct shear test on the undisturbed specimen of the soil behind the retaining wall, and then use the test results after the strain goes deep into plastic range, where strain softening occurs. Thus, it is recommended to use the residual internal friction angle ϕ_r and the residual cohesive force c_r shown in Figure 11, where $c_r = 0$.

Failure Mechanism in a Shear-Band Retaining Wall

Piping failure mechanism

Hsu *et al*. (2020) proposed a piping failure mechanism for a shear-band retaining wall, in which the shear band in the soil behind the retaining wall, after being suspended in the order of smallest to largest particle size, will flow out with the groundwater along water outlet channels (detailed in Figure 17) created by the in-series connection of pore space within the brittle-fractured shear band. Thus, this mechanism can induce piping failure in the retaining wall, as shown in Figure 18.
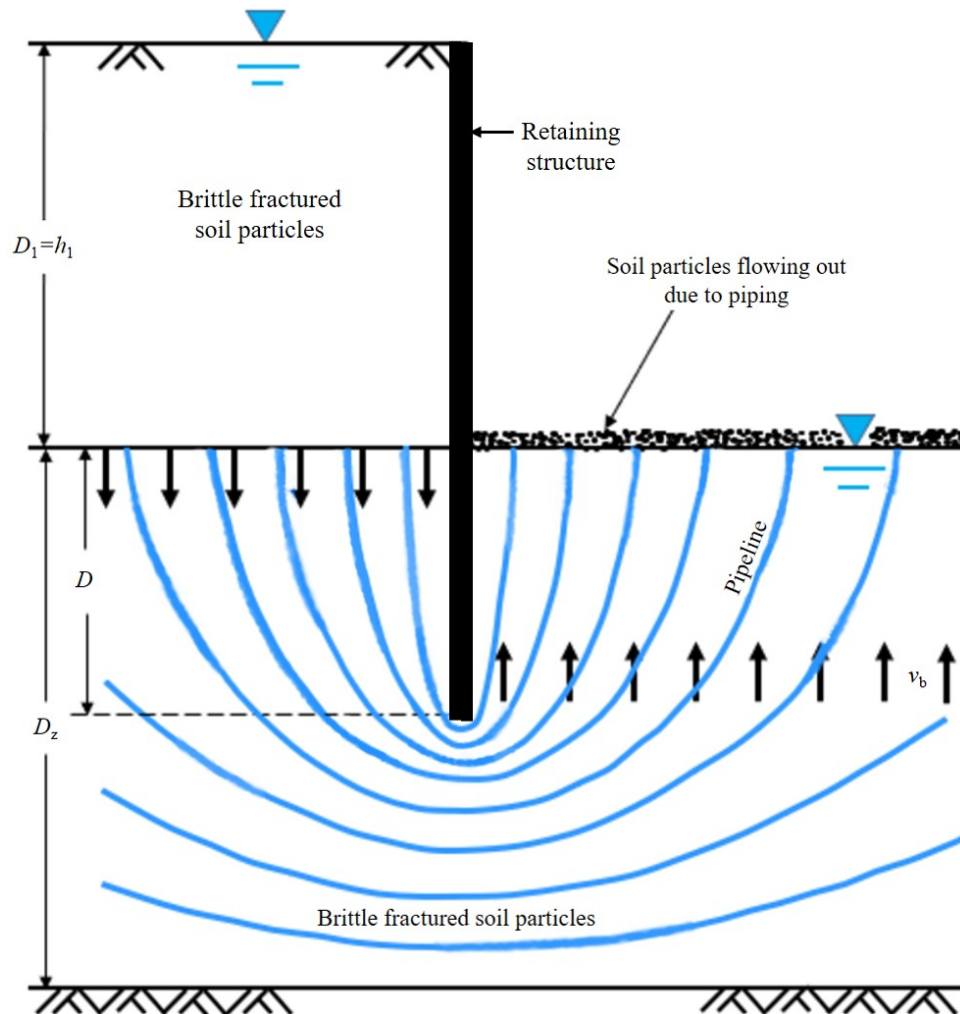
Figure 17. Schematic diagram of unsteady-state pipe flow in groundwater flowing

along pipelines in the shear band due to the difference in the groundwater

table on both sides of the retaining wall (Hsu et al., 2020).

(a) Gangweigou creek (Tainan, Taiwan; Hsu et al., 2020).

(b) Lixing Industrial Road (Nantou, Taiwan).

Figure 18. Piping failure of soils behind a retaining wall exposed to shear-banding.

According to the piping failure mechanism for a shear-band retaining wall, since the groundwater velocity in the shear band increases significantly,

the flow pattern changes from steady-state seepage flow to unsteady-state pipe flow. Therefore, the bottom velocity of the particles v_b (expressed in Equation 4) and the bottom critical velocity v_{bc} (expressed in Equation 5) required to suspend particles can be evaluated first. Piping failure in the shear-band retaining wall is defined to occur when $v_b \geq v_{bc}$ (Hsu et al., 2020):

$$v_b = \sqrt{2gh_1} \cdot E \qquad \text{(Equation 4)}$$

and

$$v_{bc} = \sqrt{\frac{2g(G_s - 1)}{1 + e}} \cdot \sqrt{D_p} \cdot \cos \beta . \qquad \text{(Equation 5)}$$

In Equations 4 and 5, g is the acceleration due to gravity, h_1 is the groundwater head difference on both sides of the retaining wall, E is the flow efficiency coefficient, G_s is the specific gravity of soil solids, e is the void ratio of the pipelines, D_p is the particle size, and β is the inclination angle of the soil deposition plane.

Strain softening failure mechanism

Figure 19(a) shows that, during the 921 Jiji earthquake, the second stepped shear banding on the left bank of the downstream Shigang Dam caused the sandy gravel behind the retaining wall to change from a dense state to a very loose state. Figure 19(b) shows that the sandy gravel slipped to the riverbed with the retaining wall after separation.

(a) Different states of sandy gravel on both sides of the failure surface.

(b) Separated sandy gravel and retaining wall slipped to the riverbed.

Figure 19. During the 921 Jiji earthquake, the collapse of the retaining wall was caused by second stepped shear banding shown in Figure 8.

Based on these findings the strain softening failure mechanism for a shear-band retaining wall can be summarized as follows:

1) Because the design code did not fortify against shear banding, the engineer applied a retaining wall design method that did not consider shear banding to a wall in a shear band zone.

2) If the soil behind a retaining wall designed for a non-shear band zone has no failure surface, and the maximum lateral earth pressure acting on the retaining wall is relatively small, the wall will not collapse.

3) If the soil behind the shear-band retaining wall has a failure surface, and the maximum lateral earth pressure acting on the retaining wall is greater than the active earth pressure calculated by traditional methods, the retaining wall is prone to col-
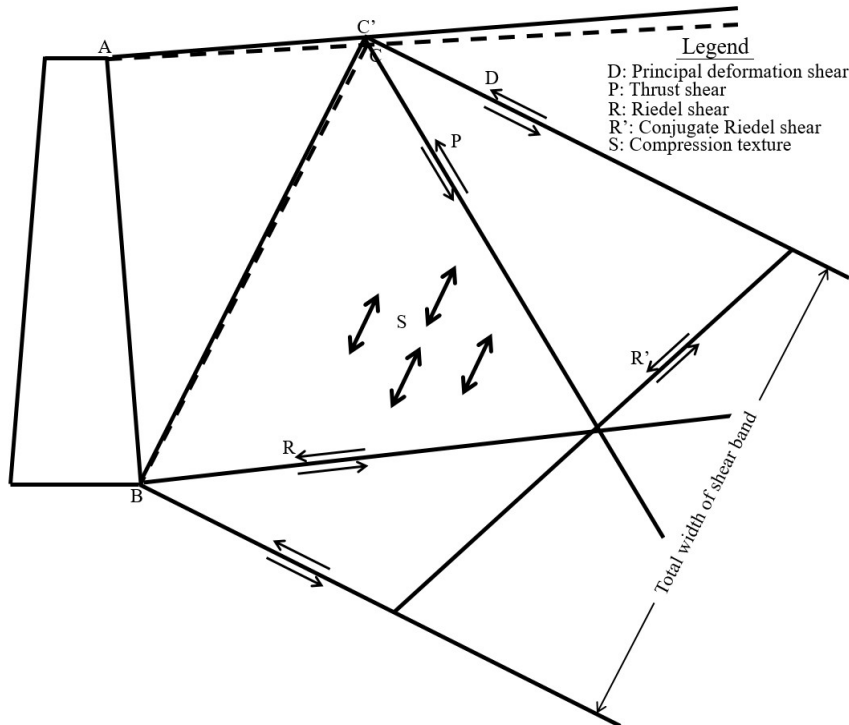
70

lapse.

4) When the failure block slides along the active failure surface, the degree of strain softening will increase with the increasing sliding speed. Therefore, the maximum lateral earth pressure on the retaining wall will continue to increase beyond the active earth pressure calculated using traditional methods, eventually causing the collapse of the retaining wall.

Shear-band tilting mechanism

Figures 6, 7, 8, and 16(c) all show

that without a vertical pressure restraint on the ground surface, the tectonic plate will induce a shear-band tilting slope under lateral compression. Figure 20(a) shows the shear-band tilting effect for a failure surface behind a retaining wall under shear banding; Figure 20(b) shows the sliding block and the sliding resistance R_s along the failure surface under the action of the shear-band tilting force P_s, and the additional maximum lateral earth pressure P_{as} in the retaining wall increased under the action of P_s; and Figure 20(c) shows the force polygon created by P_s, R_s, and P_{as}.

Legend
D: Principal deformation shear
P: Thrust shear
R: Riedel shear
R': Conjugate Riedel shear
S: Compression texture

(a) Shear-band tilting effect.

71
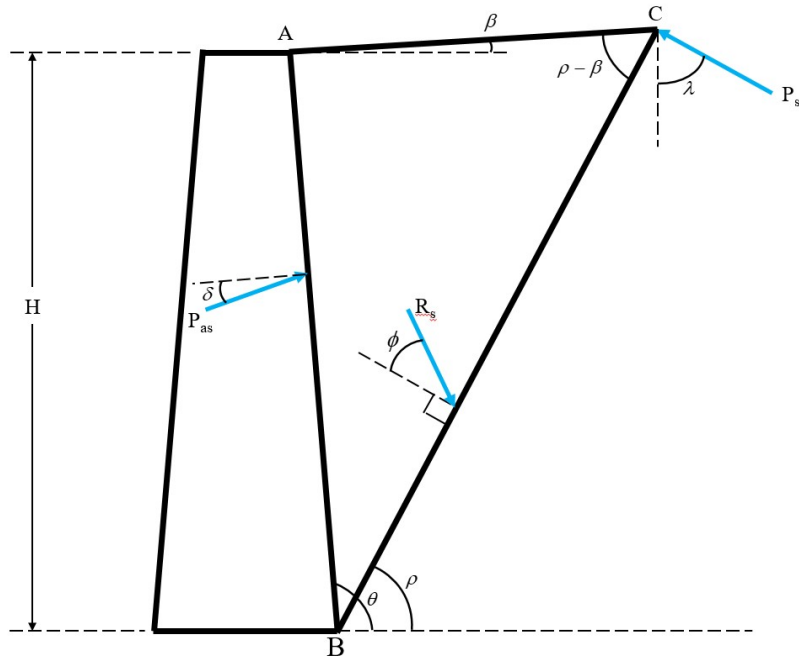
(b) Shear-banding force P_s, the resultant resistance force on the failure surface R_s,

and the lateral earth pressure increment P_{as}.
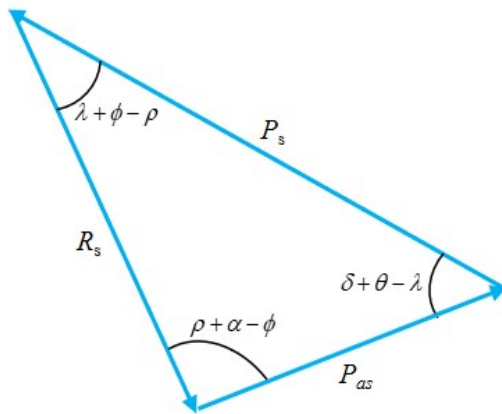
(c) Force polygon created by P_s, R_s, and P_{as}.

Figure 20. Shear-band tilting mechanism for the increase in maximum lateral earth
pressure on a retaining wall.

According to the force polygon shown in Figure 20(c) and the law of sines, P_{as} can be calculated using:

$$P_{as} = P_s \frac{\sin(\lambda + \phi - \rho)}{\sin(\rho + \alpha - \phi)}. \qquad \text{(Equation 6)}$$

Case Studies

Case 1: Piping failure of a shear-band retaining wall

For the retaining wall shown in Figure 18(b), the groundwater head difference on both sides is h_1=4 m, the acceleration due to gravity is g=9.807 m/s², the specific gravity of soil solids is G_s=2.65, and the angle of inclination in the sedimentary soil layer is β=0.

When the void ratio e=1.5, 2.0, and 2.5, the critical bottom velocity v_{bc} required to suspend soil particles with different sizes can be obtained using Equation 5, as those shown in Table 1.

Table 1. Critical bottom velocity v_{bc} for granular soil changes with the change of particle size D_p (G_s=2.65, β=0°).

Soil type	Particle size D_p	Critical bottom velocity v_{bc} (m/sec)		
		e =1.5	e =2.0	e =2.5
Silt	0.01 mm	0.011	0.010	0.010
Silt	0.05 mm	0.025	0.023	0.022
Sand	0.1 mm	0.036	0.033	0.030
Sand	0.5 mm	0.080	0.073	0.068
Sand	1 mm	0.114	0.104	0.096
Sand	5 mm	0.254	0.232	0.215
Gravel	1 cm	0.360	0.328	0.304
Gravel	5 cm	0.805	0.734	0.680
Gravel	7.5cm	0.985	0.899	0.833

Cobble	10 cm	1.138	1.039	0.962

When the pore spaces of the brittle-fractured soil exposed to shear banding are connected in series to form water outlet pipelines, the groundwater head difference on both sides of the retaining wall is h_1=4 m, the void ratio is e=1.5, and the initial efficiency coefficient is E=1%. The particle bottom velocity v_b=0.089 m/s according to Equation 4. Table 1 shows that soil fines and sand with particle sizes less than 0.5 mm are lost after being suspended in this scenario. When e increases from 1.5 to 2.0 and E increases from 1% to 5%, the bottom velocity of the particle v_b = 0.443 m/s according to Equation 4. Table 1 shows that soil fines, sand, and gravel with particle sizes less than 1 cm are lost after being suspended in this scenario. Finally, when e increases from 2.0 to 2.5 and E increases from 5% to 10%, the bottom velocity of the particle v_b=0.886 m/s according to Equation 4. Table 1 shows that soil fines, sand, and gravel with particle sizes less than 7.5 cm will be lost after being suspended in this scenario.

When soil fines, sand, and gravel in soil in a shear band behind the retaining wall continue to be lost, the shear-band retaining wall shown in Figure 18 will collapse as a result of piping effects.

Case 2: Strain softening induces an increase in the maximum lateral earth pressure in a shear-band retaining wall

In Figure 6, the retaining wall height H=6 m, the soil unit weight γ=22 kN/m^3, the internal friction angle ϕ=50°, the cohesive force c=0 kPa, the wall friction angle δ=33.3°, the inclination angle of $\overline{AC}$ β=0°, and inclination angle of $\overline{AB}$ θ=105°.

Based on this data, the inclination angle of the failure surface under elastic-perfectly plastic conditions ρ=72.83°, the weight of the failure block W= 228.46 kN, and the active earth pressure P_a=98.19 kN.

When the failure block continues to slide along the same failure surface with a failure block weight W=228.46 kN, the degrees of brittle fracture and strain softening continue to develop while the failure block slides. Thus, the internal friction angle ϕ may decrease from the peak value of 50° to the residual value of 33° (McCarthy, 1977),

74

and the wall friction angle δ may decrease from 33.3° to 22°. The maximum lateral earth pressure P_a on the retaining wall, shown in Table 4, can be calculated using Equation 2. According to Table 4, it is clear that the maximum lateral earth pressure on the retaining

wall continues to increase beyond the active earth pressure calculated by traditional methods as the starting point, and the maximum increase in the maximum lateral earth pressure is up to 48.32 kN.

Table 4. Analysis results for the increased maximum lateral earth pressure induced by strain softening for the shear-band retaining wall.

$\phi_p \rightarrow \phi_r$	δ	P_a(kN)	ΔP_a(kN)
$50°\rightarrow36°$	$33.3°\rightarrow24°$	98.19→137.05 (100%→139.6%)	38.86
$50°\rightarrow33°$	$33.3°\rightarrow22°$	98.19→146.51 (100%→149.2%)	48.32
$40°\rightarrow36°$	$26.7\rightarrow24°$	125.36→137.05 (100%→109.3%)	11.69
$40°\rightarrow33°$	$26.7\rightarrow22°$	125.36→146.51 (100%→116.9%)	21.15

Note: ϕ_p was taken from McCarthy (2007), and let ϕ_r be equal to $\frac{2}{3}\phi_p$.

Case 3: Shear-band tilting effect induces an increase in the maximum lateral earth pressure on a shear-band retaining wall

In this case, the same retaining wall as in Case Study 2 is used. Therefore, under the elastic-perfectly plastic condition, the calculated inclination angle of the failure surface ρ =72.83°, the weight of the failure block

W=228.46 kN, and the active earth pressure P_a =98.19 kN. These results are the same as in Case 2.

When one side of the failure block is lifted as a result of the shear-band tilting effect, the tilting force P_s can be increased from 0.5W (slow shear banding) to 1.0W (rapid shear banding). Equation 4 can be used to calculate the increase in the maximum lateral earth

75

pressure P_{as} on the retaining wall that is induced by the shear-band tilting force. It is found that P_{as} was greater compared with the traditional active earth pressure (P_a =98.19 kN) as P_{as} increased from 48.81 kN to 97.62 kN. Therefore, P_{as} increased by a maximum percentage of 99.4%.

Comparison and Discussion of Results

1) In the past, engineers used the mechanism proposed by Terzaghi (detailed in Figure 23), the father of soil mechanics, to analyze the piping failure potential of retaining walls. For the retaining wall shown in Figure 21, Terzaghi (1943) proposed a safety factor against piping,

$FS = W'/U_s$, where

$W' = (\gamma_{sat} - \gamma_w)D^2/2$,

$U_s = h_{ave}\gamma_w D/2$, γ_{sat} is the unit weight of saturated soil, γ_w is the unit weight of water, h_{ave} is the average seepage head at the bottom of a potential piping block, and D is the depth of the embedded sheet pile. According to this method, piping failure occurs when FS ≤ 1.0. Therefore, in Case Study 1, when h_1=4 m, G_s=2.65, e=1.5, γ_w=9.81 kN/m^3, γ_{sat}=16.28 kN/m^3, D=3 m, and h_{ave}=1.5 m (detailed in Figure 18(b)), the calculated FS=1.32. According to Terzaghi's definition, since FS>1.0, piping failure will not occur in the retaining wall.
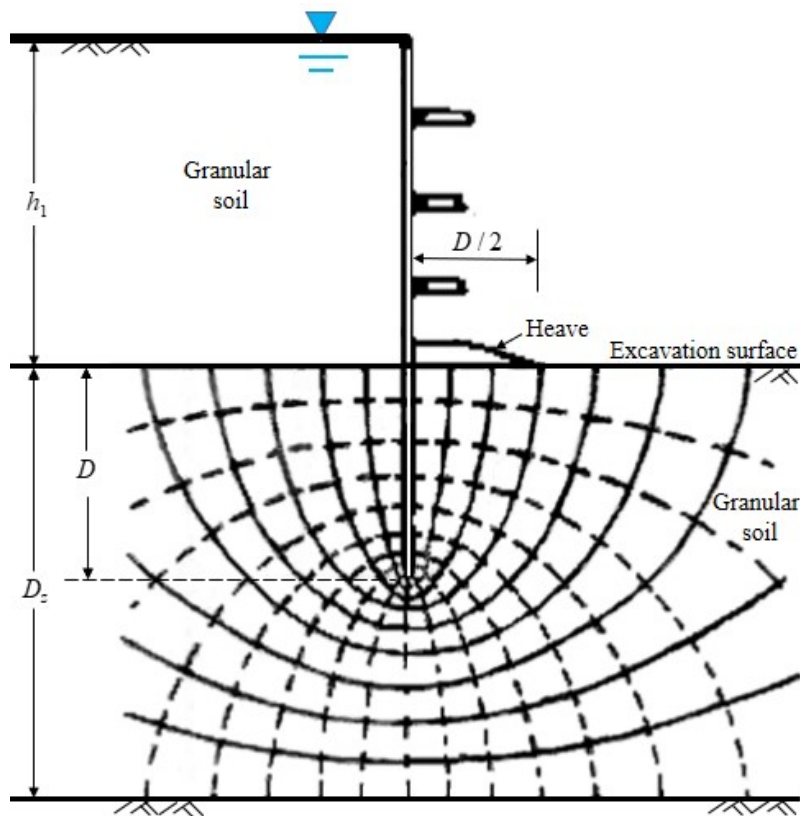
(a) Steady-state seepage flow grid.
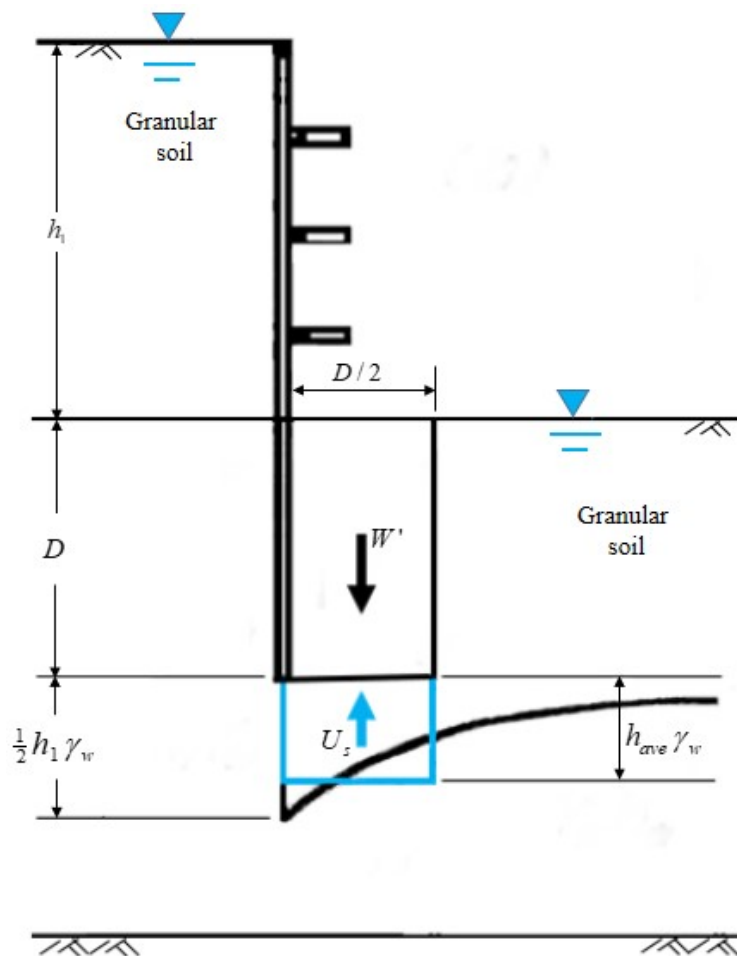
(b) W' and U_s, which are required to calculate the piping resistance safety factor.

Figure 21. Piping failure mechanism proposed by Terzaghi (1943).

It can be seen that, in the case where piping failure has occurred, the piping failure cannot be determined based on the piping failure mechanism proposed by Terzaghi. Therefore, if the analysis for assessing piping failure in a retaining wall is to meet real design needs, then the unsteady-state pipe flow mechanism proposed by Hsu *et al.* (2020) should be adopted rather than the steady-state seepage flow mechanism proposed by Terzaghi (1943).

2) The traditional theory of active earth pressure on retaining walls is based on the elastic-perfectly plastic model (detailed in Figure 15(b)), which assumes that the active failure surface occurs when the shear stress of the soil behind the retaining wall

reaches the limit shear resistance strength without being proven. However, observations show that the active failure surface only develops after the strain goes deep into the plastic range and strain softening occurs. Therefore, the traditional theory of active earth pressure on retaining walls does not meet the real needs of retaining walls.

3) When analyzing the maximum lateral earth pressure on the retaining wall, the internal friction angle ϕ under the limit condition for non-cohesive soil, or the internal friction angle ϕ and the cohesion c under the limit condition for cohesive soil are used. However, the active failure surface only appears when the strain goes deep into the plastic range and strain softening occurs. In this case, the internal friction angle of the soil behind the retaining wall approaches the residual internal friction angle ϕ_r, and the cohesion also approaches the residual cohesion c_r, where $c_r = 0$. Therefore, according to the internal

friction angle ϕ of the non-cohesive soil under the limit condition, or to the cohesive force c and the internal friction angle ϕ of the cohesive soil, the analysis for the maximum lateral earth pressure on the retaining wall shows that the wall does not meet the real needs of a retaining wall in the existence of a failure block.

4) Figure 22(a) shows that the retaining wall was locally subjected to a two-way shear-band tilting effect during the 921 Jiji earthquake. Although the retaining wall locally collapsed in the shear band, the soil behind the retaining wall remained on the river bank. Moreover, the entire retaining wall adjacent to the site of local collapse did not collapse because it was unaffected by the shear-band tilting effect. Therefore, it can be concluded that a retaining wall that meets existing design specifications will only collapse as a result of the strain softening and shear-band tilting effects induced by shear banding.

(a) Soil behind the retaining wall remained on the river bank
after the retaining wall collapsed.

(b) Bidirectional shear-band tilting effect on the soil
behind the collapsed retaining wall

Figure 22. Local collapse of a retaining wall under shear banding.

5) When strain softening occurs in the soil behind a retaining wall, the maximum lateral earth pressure increases beyond the traditional active earth pressure as the starting point. The results of Case 2 show that the strain softening effect can cause the maximum lateral earth pressure on the retaining wall to increase up to 49.2%. The results of Case 3 show that the shearing banding force can cause the maximum lateral earth pressure of the retaining wall to increase up to 99.4%. Shear banding induces strain softening and the shear-band tilting effect, and these two effects can be superimposed; therefore, under shear banding, the

81

maximum lateral earth pressure on the retaining wall will increase by an additional 148.6%. These results quantitatively show that a retaining wall that meets the existing design code will only collapse as a result of the strain softening and shear-band tilting effects induced by shear banding.

Conclusions and Suggestions

A large number of retaining walls on highway slopes and river banks have been built, and these walls were traditionally designed according to the active earth pressure theory that was proposed by Coulomb in 1776. However, since the development of this theory, scholars have continued to put forward relevant research results. Traditional active earth pressure theories for retaining wall design are all based on the elastic-perfectly plastic model. The maximum lateral earth pressure on the retaining wall obtained by limit analysis is defined as the active earth pressure, which is used as the fortification basis for current retaining wall design codes. According to the models, retaining walls that meet the design codes should remain stable throughout their design life. However, a large number of retaining walls have experienced local collapse in the shear band during their service lives.

In view of this, the main cause for the collapse of shear-band retaining walls was proved in this paper. Using the results of finite-element analysis and case studies, the following four conclusions are made:

1) For a retaining wall that meets the design specifications, the mechanism proposed by the authors can be used to explain the local collapse of a retaining wall because the three criteria for identifying the main cause showed that the current design code does not fortify against shear banding.

2) When there is a height difference between the groundwater table on both sides of the shear-band retaining wall, the soil particles behind the retaining wall will become suspended in the order of the smallest to largest particle size. These particles can then flow out with the groundwater along outlet pipelines formed by connected pore spaces in a brittle-fractured shear band. Therefore, to obtain analysis results that are consistent with the piping failure potential of the actual shear-band retaining wall, the unsteady-state pipe flow mechanism must be used instead of the steady-state seepage flow mechanism.

82

3) A finite-element simulation analysis of a tectonic plate under lateral compression was conducted. The results showed that shear bands will only appear in the tectonic plate under the elastic-plastic strain softening model. However, the traditional active earth pressure theory for retaining walls, which is based on the elastic-perfectly plastic model, does not meet the real needs of retaining walls without inducing a failure surface.

4) Both strain softening and shear-band tilting effects will further increase the maximum lateral earth pressure on the shear-band retaining wall compared with the traditional active earth pressure as the starting point. When strain softening and the shear-band tilting effect are superimposed under shear banding, the increase in the maximum lateral earth pressure on the retaining wall will increase by an additional 148.6%, showing that these effects are key factors in the collapse of shear-band retaining walls.

Based on the above four conclusions, the following two suggestions are made:

1) The maximum lateral earth pressure on the retaining wall according to the elastic-plastic strain softening model is much greater than the active soil pressure according to the elastic-perfectly plastic model. To ensure the stability of the shear-band retaining wall, it is recommended to use the maximum lateral earth pressure according to the elastic-plastic strain softening model when designing retaining walls for shear banding, instead of the maximum lateral earth pressure according to the elastic-perfectly plastic model.

2) Since different test methods use different stress paths to test specimen failure, it is recommended to use the direct shear test with a horizontal displacement exerted by the side of the upper or lower box of the square shear box instead of the traditional compression test, in which vertical pressure is applied to the upper and lower surfaces of a cylindrical specimen.

References

Ahire1, D., Baviskar1, P., Manghani1, J., Madankar1, B., Patil1, D., "Seismic Earth Pressure Analysis of Retaining Wall," International Journal for Research in Engineering Application & Management (IJREAM) *ISSN: 2454-9150,* Vol. 5, No. 2, 2019.

Bowles, Joseph E., "11-6 Active and Passive Earth Pressure Using Theory of Plasticity," Foundation Analysis and Design, 4th Edition, McGraw-Hill Book Company, pp. 489-493, 1988.

Chen, Wai-Fah., "Chapter 2 Assumption and Theorems in Limit Analysis," *Limit Analysis and Soil Plasticity*, Developments in Geotechnical Engineering 7, 1975.

China Earthquake Disaster Prevention Center, What Is Earthquake - Type of Earthquake, China Digital Science and Technology Museum: Talk about Earthquake, Website: http://amuseum.cdstm.cn/AMuseum/earthquak/1/2j-1-2.html, 2019.

Coffey, J., "What are the Different Types of Earthquakes?" Universe Today, Space and astronomy news, Website: https://www.universetoday.com/82164/types-of-earthquakes/, 2019.

Coulomb, C. A., "Essai sur une application des regles des maximis et minimis a quelques problemes de statique relatifs a l'Architecture," Memoires de Mathematique et de Physique, Presentes a l'Academie Royale des Sciences, par divers Savans, et lus dans ses Assemblees, Paris, Vol. 7, (volume for 1773), pp. 343-382, 1776.

Google Earth, Website: http://www.google.com.tw/intl/zh-tw/earth/, 2010.

Hsu, Tse-Shan, *Capturing Localizations in Geotechnical Failures*, Ph. D. Dissertation, Civil Engineering in the School of Advanced Studies of Illinois of Technology, p. 105, 1987.

Hsu, Tse-Shan, "Chapter 3: The Major Cause of Earthquake Disasters: Shear Bandings," *Earthquakes-Forecast, Prognosis and Earthquake Resistant Construction*, Edited by Valentina Svalova, IntechOpen, pp. 31-48, Website: https://www.intechopen.com/books/earthquakes-forecast-prognosis-and-earthquake-resistant-construction/the-major-cause-of-earthquake-disasters-shear-bandings, 2018.

Hsu, Tse-Shan, *Introduction to Tectonic Earthquake Resistant Performance Design*, Feng-Chia University, Taiwan, 2019.

Hsu, Tse-Shan, Chen, Yi-Ju, Wu, Zong-Lin, Chao, Tzu-Che, Wei, Ding-Yu, Yang, Jiann-Cherng

84

Huang, Yi-Min, "overning Equations and Complete Mathematical Proofs for Coulomb's Theory of Earth Pressure," *International Journal of Organizational Innovation*, Volume 13, No, 4, pp. 1-20, 2021.

Hsu, Tse-Shan, Chen, Ming-Tuo, Chiu, Shey-En, "The Major Cause for the Destruction of the Gangweigou Creek Floodway," *The International Journal of Organizational Innovation*, Vol. 13, No. 2, pp. 120-143, 2020.

Hvorslev, M. J., "Physical Components of the Shear Strength of Saturated Clays," Research Conference on Shear Strength of Cohesive Soils, ASCE. pp. 169-273. 1961.

Lambe , T. William and Whitman, Robert V., **Soil Mechanics**, John Wiley & Sons, New York, pp. 65, 1969.

Lian, Yong-Wang, *Crack of the Earth*. Professional Aerial Photography, Feihu Cultural Enterprise Co., Ltd., Taichung, 1999.

McCarthy, D. F., *Essentials of Soil Mechanics and Foundations*, 7th Edition, New Jersey, Prentice Hall, p. 399, 1977.

Needleman, A., and Tvergaard, V., "Finite Element Analysis of Localization in Plasticity," in *Finite Elements: Special Problems in Solid Mechanics*, Vol. 5, ed. Oden, J. T., and Carey, G. F., Prentice-Hall. Inc.. Englewood Cliffs, New Jersey, pp. 94-157, 1983.

New Taipei City Government, Taiwan, *The Lincoln Mansion Disaster Victims*, 1997.

Prevost, J. H., "Short Communication: Localization of Deformations in Elastic-Plastic Solids," *International Journal for_Numerical and_Analytical Methods in Geomechanics*, Vol. 3, pp. 187-196, 1984.

Rice, J. R., "The Localization of Plastic Deformation," *Proceedings of the 14th International Congress on Theoretical and Applied Mechanics*, Delft, 1976, ed. W.T. Koiter, North Holland, Amsterdam, Vol. 1, pp. 207-220, 1976.

Rudnicki, J. W. and Rice, J. R., "Conditions for the localization of deformation in pressure-sensitive dilatants materials," *Journal of the Mechanics and Physics of Solids*, Vol. 23, pp. 371-394, 1975.

85

Sitar1, N., Wagner, N., "On Seismic Response of Stiff and Flexible Retaining Structures," *6th International Conference on Earthquake Geotechnical Engineering*, Christchurch, New Zealand, Website: https://www.issmge.org/publications/online-library, 2015.

Tchalenko, J. S., "The evolution of kink-bands and the development of compression textures in sheared clays", *Tectonophysics*, Volume 6, pp. 159-174, 1968.

Terzaghi, K., *Theoretical Soil Mechanics*, John Wiley & Sons, Inc., pp. 257-262, 1943.

Terzaghi, Karl; Peck, Ralph B.; Mesri, Gholamreza, "28. Rankine's earth-pressure theory" *Soil mechanics in engineering practice*, 3rd ed., New York: Wiley. pp. 246–249, 1996.

Valanis, K. C., "Banding and stability in plastic materials," *Acta Mech*, Vol. 79, pp. 113-141, 1989.

Water Resources Department Newsletter, Website: http://epaper.wra.gov.tw/Article_Detail.aspx?s=CCD4A9BADAEA6D38, 2018.